Development of Kinetics for Soot Oxidation at High Pressures Under Fuel-Lean Conditions

JoAnn S. Lighty
Department of Chemical Engineering, University of Utah, jlighty@utah.edu
Randall Vander Wal
Dept. of Energy and Mineral Engineering, Pennsylvania State University, ruv12@psu.edu

Project Scope

The focus of the proposed research was to develop kinetic models for soot oxidation with the hope of developing a validated, predictive, multi-scale, combustion model to optimize the design and operation of evolving fuels in advanced engines for transportation applications. The work focused on the relatively unstudied area of the fundamental mechanism for soot oxidation. The objectives include understanding of the kinetics of soot oxidation by O_2 under high pressure which require: 1) development of intrinsic kinetics for the surface oxidation, which takes into account the dependence of reactivity upon nanostructure and 2) evolution of nanostructure and its impact upon oxidation rate and 3) inclusion of internal surface area development and possible fragmentation resulting from pore development and /or surface oxidation. These objectives were explored for a variety of pure fuel components and surrogate fuels.

This project was a joint effort between the University of Utah (UU) and Pennsylvania State University (Penn State). The work at the UU focuses on experimental studies using a two-stage burner and a high-pressure thermogravimetric analyzer (TGA). Penn State provided HRTEM images and guidance in the fringe analysis algorithms and parameter quantification for the images. This report focuses on completion done under supplemental funding.

Findings

The results of the oxidation studies can be summarized in two different sections.

1. Oxidation of soot derived from liquids fuels
2. Oxidation of model carbons

1. Oxidation of soot derived from liquid Fuels

1.1 Soot oxidation kinetics

The study of the oxidation kinetics of soot samples obtained from different liquid fuels, both oxygenated fuels and jet fuels, and two standards (a commercial black carbon sample and a reference diesel soot) was performed under different pressures. The experiments were conducted using pure n-dodecane, m-xylene, and a mixture of the two. n-butanol was used as oxygenated fuel and n-dodecane with the addition of butanol was used as a surrogate for an oxygenated diesel.

Soot samples from the liquid fuels previously mentioned were generated in a flat-flame, premixed burner under heavily-sooting conditions and captured on a water-cooled stabilization plate located above the burner surface. The collected soot was oxidized using a high-pressure Thermogravimetric Analyzer (HTGA). The TGA operation was optimized to reduce mass transfer effects by adjusting the oxidizer flow rate and initial sample mass. Further corrections for mass transfer were accomplished by computing the effectiveness factors for intraparticle, interparticle, and external mass transfer. Two pressures were evaluated (1 and 10 atm) and O_2 concentration was varied between 10 and 21%. Tables 1 to 3 show the results of this part of the study. Results showed that there was not a significant difference in the activation energies of the soot samples for either pure components or as a mixture, with exception of

soot from oxygen-containing fuels. in addition, pressure did not change the activation energies when mass transfer corrections were applied.

Table 1 presents the results of the kinetic parameters after mass transfer limitation corrections were applied for the carboxen and m-xylene/n-dodecane samples. The activation energies were nearly the same for the 1 and 10 atm experiments.

Table 1. Kinetic parameters after mass transfer limitation corrections were applied.

	1 atm		10 atm	
Soot sample	**Ea (kJ/mol)**	**R^2**	**Ea (kJ/mol)**	**R^2**
carboxen	141± 6	0.98	144± 7	0.99
m-xylene/n-dodecane[a]	161± 4	0.99	159± 5	0.98

[a] mixture consist of 83 mol% *n*-dodecane and 17 mol% *m*-xylene

Table 2 presents the soot-oxidation kinetic parameters obtained in this study. These parameters were calculated from the TGA mass loss curves under isothermal conditions together with an Arrhenius-type equation. As listed in Table 2 for the m-xylene, n-dodecane, and the mixture, the activation energies were quite similar with a range from 154 to 165 kJ/mol. There was not a significant difference between the pure component fuels and the mixture. The activation energies for reference diesel soot and commercial black carbon were 139 and 141 kJ/mol respectively. The activation energy values for different soot samples under atmospheric conditions were in the range reported in the literature [1-8] for experiments where kinetics control the reaction. The activation energy for standard carboxen was also in the range previously reported by Sorensen et al.[9].

Table 2. Kinetic parameters extracted from Arrhenius plots for the different soot samples.

Soot sample	**% O_2**	**T range (°C)**	**Ea (kJ/mol)**	**A ($pa^{-1}min^{-1}$)**	**R^2**
m-xylene	10	550-625	160± 5	2.63E+05	0.91
m-xylene	15	400-625	160±6	9.87E+04	0.99
m-xylene	21	550-650	161±7	2.53E+05	0.98
n-dodecane	10	550-650	162±5	9.93E+04	0.98
n-dodecane	15	400-625	159±4	2.96E+05	0.96
n-dodecane	21	550-625	165±5	5.58E+05	0.98
m-xylene/n-dodecane	10	550-625	161±4	3.04E+05	0.99
m-xylene/n-dodecane	15	400-625	154±5	6.95E+05	0.97
m-xylene/n-dodecane	21	550-625	158±6	1.63E+05	0.98
Carboxen	21	550-650	141±4	1.86E+03	0.94
Standard diesel	21	575-675	139±3	7.40E+02	0.96

Table 3 presents the kinetic parameters extracted from Arrhenius plots for the oxygenated diesel and n-butanol fuels. The activation energy values were 114 kJ/mol for n-butanol and 129 kJ/mol for the mixture of n-butanol/n-dodecane. These activation energies were lower than those estimated with the fuels listed in Table 2.

Table 3. Kinetic parameters extracted from Arrhenius plots for n-butanol and n-butanol/n-dodecane.

Soot sample	E_a (kJ/mol)	R^2
n-butanol/n-dodecane	129±4	0.98
n-butanol	114±3	0.96

1.2 Soot nanostructure

Soot nanostructure for the soot collected from the flat flame "nascent", and partially oxidized at 1, 10 and 40 atm was studied by High-Resolution Transmission Electron Microscopy (HRTEM). The lattice fringe length and fringe tortuosity were estimated to correlate the nanostructure with the soot reactivity.

The HRTEM images for each of the nascent soot samples are shown in Figure 1. From the figure it is possible to visualize that the nascent soot nanostructure was quite similar across the different fuels

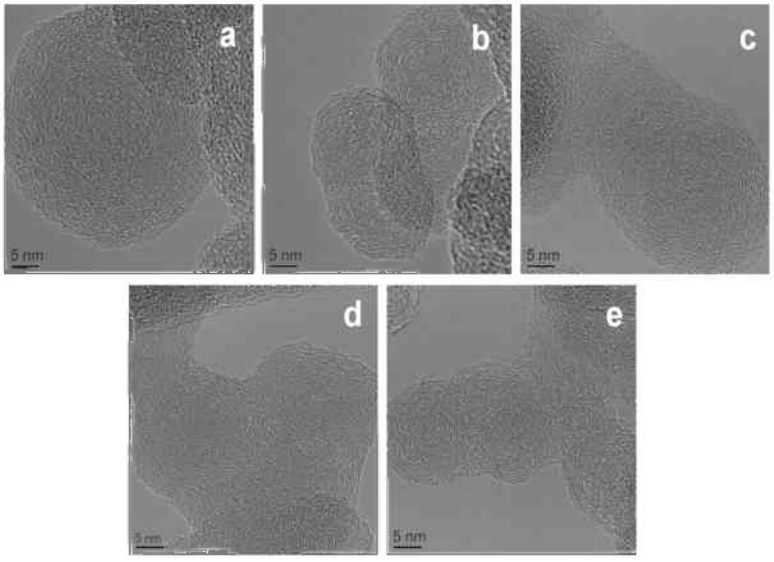

Figure 1. Representative HRTEM images of nascent soot for the fuels: (a) n-butanol/n-dodecane, (b) n-butanol, (c) n-dodecane, (d) m-xylene/n-dodecane, and (e) m-xylene.

The image quantification by lattice fringe analysis was performed to obtain statistical metrics (fringe length and tortuosity) which describe the nanostructure order.

Figure 2. shows the extracted lamellae length and tortuosity distributions across the five different fuels. The distributions were quite similar across the different fuels with the n-butanol/n-dodecane distributions showing only a slightly longer tortuosity and smaller fringe length.

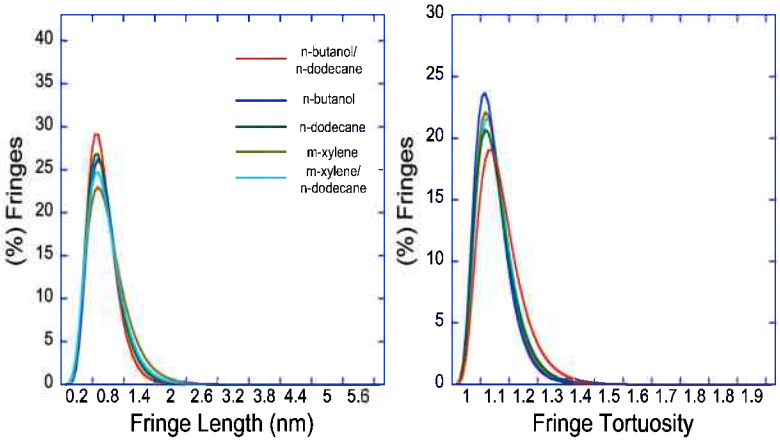

Figure 2. Extracted fringe length and fringe tortuosity histograms for the nascent parent fuel. The PDFs are lognormal distributions.

The HRTEM images of partially oxidized (extent 50%) soot across the different fuel components and blends at pressures of 1 atm, 10 atm, and 40 atm showed that core-shell structures [10, 11] were predominantly found in most of the samples, with this term denoting a marked difference in nanostructure between the interior and outer portion of the particles. The fringe analysis on these images was obtained and shown in Figure 3.

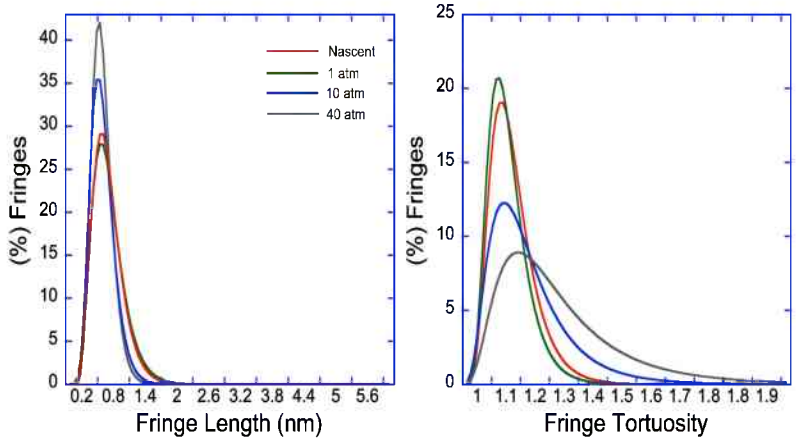

Figure 3. (a) Fringe length histograms, (b) Fringe tortuosity histograms for the fuel mixture n-butanol/n-dodecane.

Fringe-length and tortuosity histograms are shown separately in Fig. 3 for the n-butanol/n-dodecane mixture. Across the oxidation series there was a progressive decrease in structure for the n-butanol/n-dodecane soot, as manifested by the narrowing of the fringe length distribution and a broadening of the complimentary tortuosity distributions.

Surface carbon oxidation studies by X-ray photoelectron spectroscopy (XPS) were carried out to understand the differences in reactivity of the fuels studied. Figure 4 summarizes the sp^2/sp^3 ratio values across nascent soots from the different fuel blends.

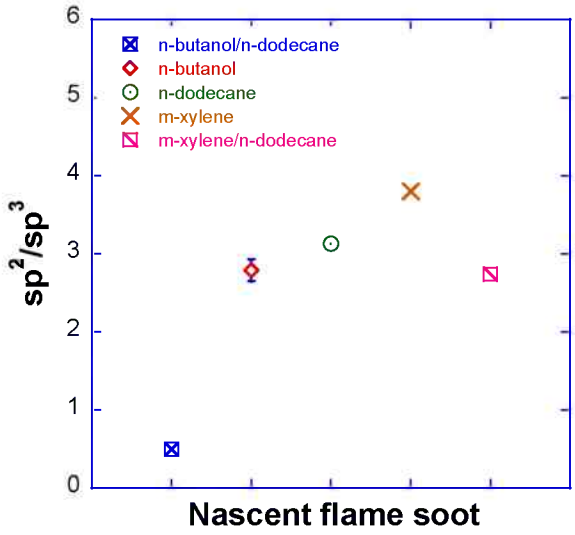

Figure 4. The sp^2/sp^3 values (derived from XPS) for different nascent fuel components and blends, representative error bar shown.

As shown, the pure fuel components and their blend (m-xylene/n-dodecane) exhibited similar (higher) sp^2/sp^3 ratio values, while the sp^2/sp^3 ratio of soot from the oxygenated fuel blend (n-butanol/n-dodecane) was significantly lower (by a factor of ~6). Notably, the oxygenated fuel blend contains considerable organic content, as evidenced by the large sp^3 component; similar composition was observed elsewhere in biodiesel derived soots [12].

in order to establish a relation between HRTEM results and the reactivity, the fringe length and the fringe tortuosity for the different nascent soot samples, are plotted against the activation energy values (see Figure 5). Similarity of fringe length values for the nascent soots make challenging a definitive interpretation of E_a values as reflecting initial nanostructure, as reflected in the plots shown in Figure 5.

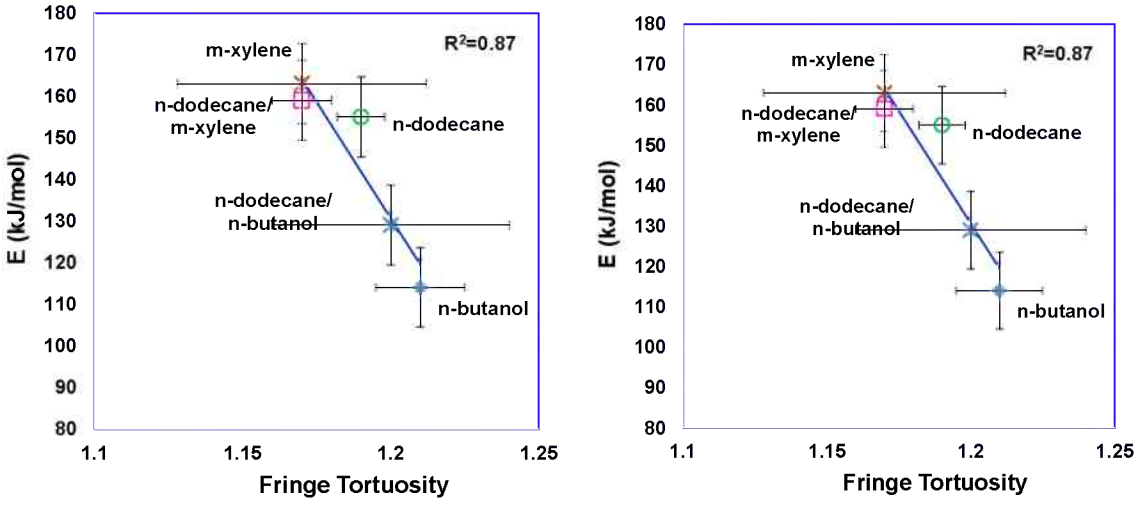

Figure 5. Activation Energy vs. Fringe analysis parameters, a) Fringe length, b) Fringe tortuosity, representative error bar shown.

While previous studies have shown such dependence, those studies also benefited from a diversity of nascent nanostructures, in contrast to the present set. The second part of this study, using model carbons, helped resolve such dependencies.

2. Oxidation of Model Carbons

2.1 Soot Oxidation kinetics

Oxidation kinetics and fringe analysis studies of three "model" carbons, ranging from amorphous to onion-like nanostructures and a reference diesel soot were performed in a Thermogravimetric Analyzer (TGA). The samples were oxidized isothermally at temperatures ranging from 575 to 775 °C in air. Multiple tests were performed to obtain the most favorable operating conditions to minimize mass-transfer diffusion limitations in the experiments.

An Arrhenius-type equation and first-order reaction kinetics was used to extract the kinetic parameters. The activation energies for the oxidation of the carbon samples range from 124 to 204 kJ/mol, and it was approximately 140 kJ/mol for the reference diesel soot sample. The onion-like structure exhibited a slower kinetic rate compared to the amorphous M1300 as shown in Figure 6. Similar kinetic parameters were found for R-250 and reference diesel soot samples. The activation energies obtained for the samples studied were in accordance with data reported in the literature for carbon blacks and diesel soot samples [3, 6,13-15].

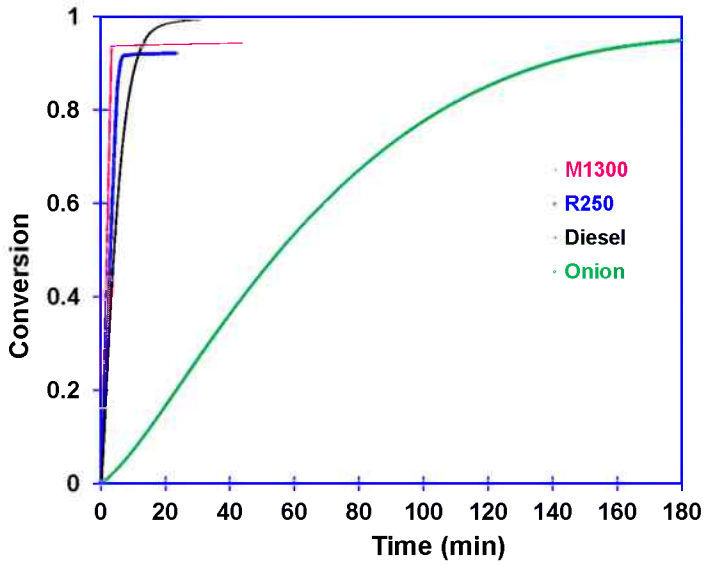

Figure 6. Mass-based oxidation rate for three different carbon black samples and diesel sample, at 600 °C in air.

2.2 Soot nanostructure

Upon partial oxidation (extent 50%), HRTEM was performed to examine the nanostructural changes relative to the nascent material, and also to study the pressure dependence.

HRTEM images of the three carbon blacks and the diesel soot were obtained and presented in Figure 7. in these images, M1300 exhibits mostly partially and completely closed shells whose diameter is roughly a few nanometers. In most cases the shells are not spherical but distorted, with the interior of these shells appearing to be a void. in contrast, R250 has short, disconnected, planar crystallites comprising several polyaromatic hydrocarbon layers that are oriented concentrically. The particle interior was more spatially

disorganized carbon. The OLC exhibited extended carbon lamella, many of which are oriented parallel to each other. This organization is characteristic of a crystallite structure. Dissimilar to the carbon blacks, the reference diesel soot showed a core shell structure.

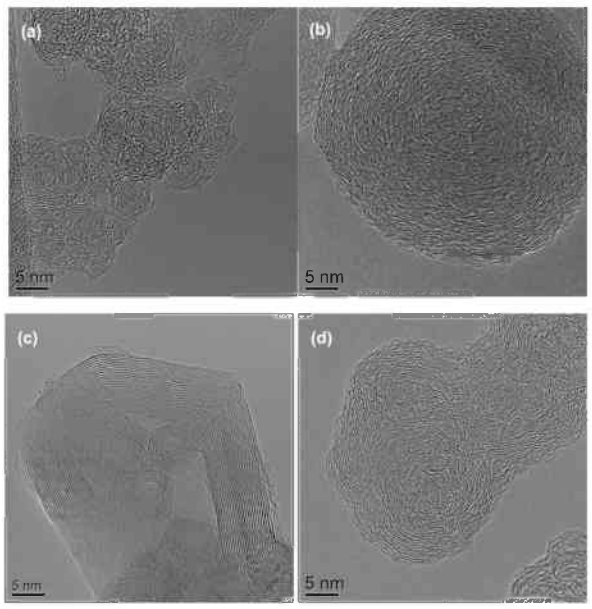

Figure 7. HRTEM images of different nascent samples, a) M1300, b) R 250, c) OLC, and d) diesel soot.

Results of the partial oxidation (extent 50%) samples showed that for M1300 (see Figure 8) still consists of partially formed shells, but many of which have transformed to extended lamellae with no visible voids. Both the pressure conditions (1 and 10 atm) showed roughened surfaces that are indicative of oxidation.

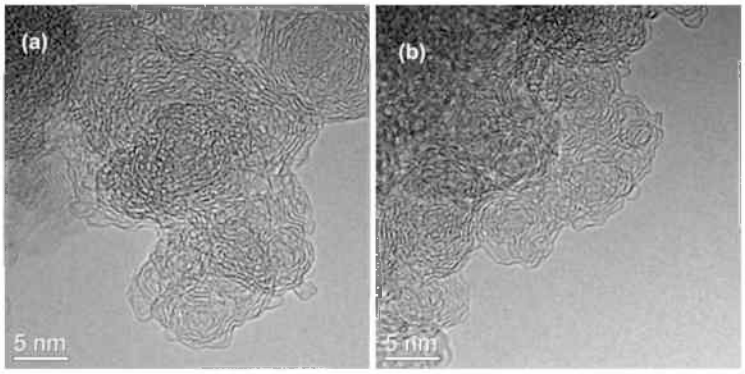

Figure 8. Representative HRTEM images of partially oxidized (50%) M1300, a) 1 atm and b) 10 atm.

In contrast, R250 carbon black exhibited noticeably different nanostructure compared to the nascent nanostructure as shown in Figure 9. At atmospheric pressure, the extended lamella at the particle perimeters is observed in the images. Hollow shell-like particles appear together within aggregates. The lamellae on the particle perimeters were not highly ordered, but it was more undulated. This different burning mechanism was earlier reported for diesel soots, but it is a unique observation for R250 [16-18].

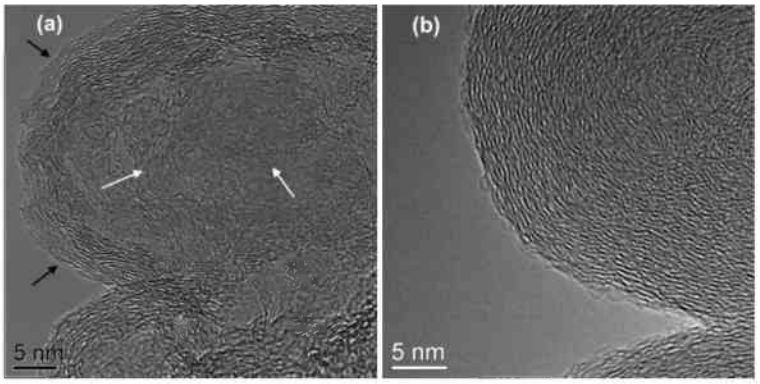

Figure 9. Representative HRTEM images of partially oxidized (50%) R250, a) 1 atm and b) 10 atm. White arrow shows hollow shell, black arrow indicates lamellae on the particle perimeter.

The surface oxidation caused by internal burning enabled nanostructure development under atmospheric pressure conditions. This variation in nanostructure was not observed when R250 was oxidized at a higher pressure (10 atm). The mass transfer diffusion limitations (as observed from the TGA data) might have played a crucial role under higher pressure conditions.

With increasing oxidative pressure, OLC exhibited a decrease in graphitic structure and increase in curvature primarily because of outer surface breakup (see Figure 10).

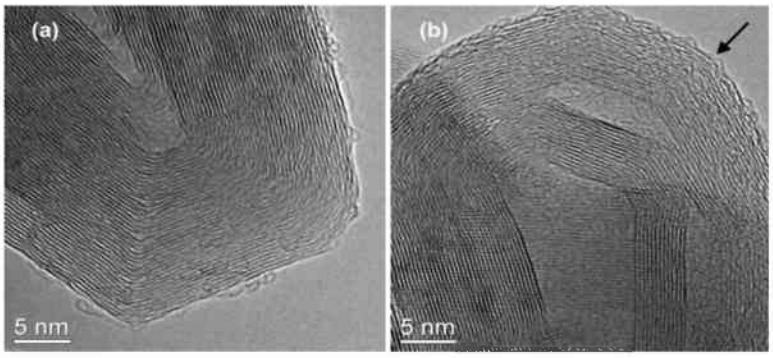

Figure 10. Representative HRTEM images of partially. oxidized (50%) OLC, a) 1 atm and b) 10 atm .Black arrow indicates lamellae on the particle perimeter.

Similar to the R250, diesel soot also showed different burning modes at the two oxidative pressures studied. HRTEM images for diesel soot are presented in Figure 11.

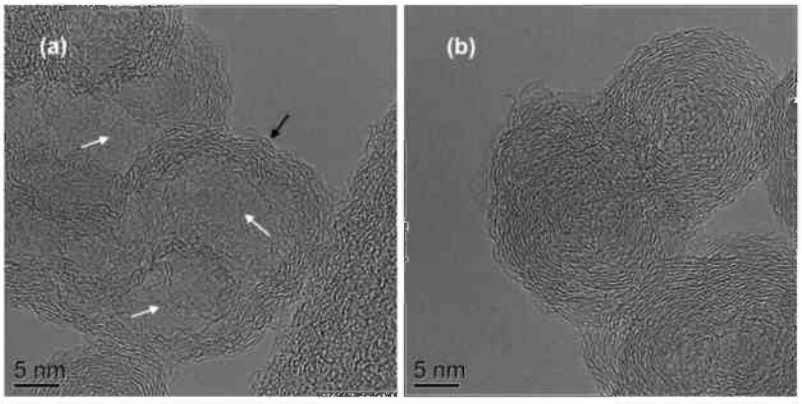

Figure 11. Representative HRTEM images of partially oxidized (50%) diesel, a) 1 atm and b) 10 atm.

The median fringe length and tortuosity values are summarized in Figure 12, for the three carbon blacks and diesel soot at nascent and oxidation pressure conditions.

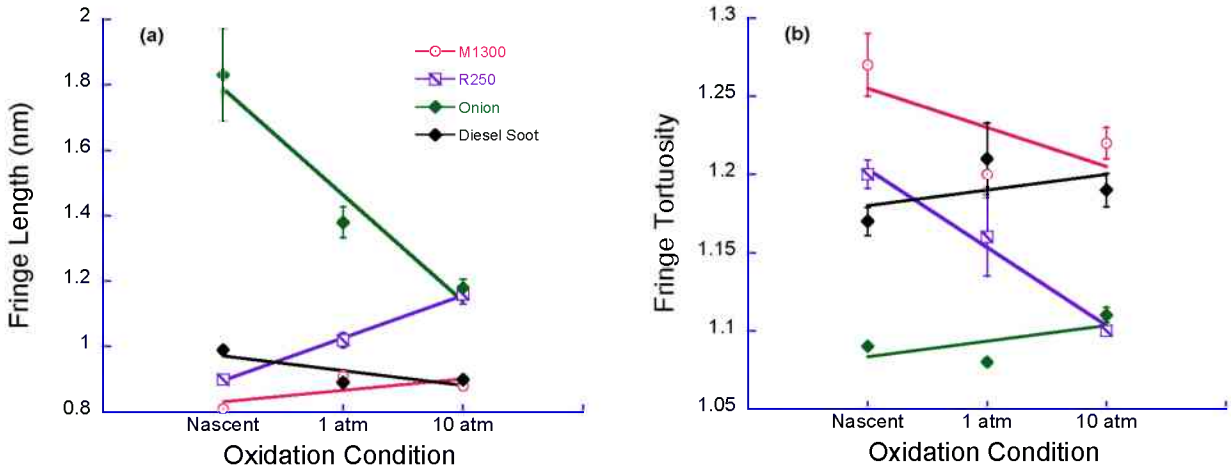

Figure 12. Comparison of the median (a) fringe length and (b) tortuosity extracted from the lognormal distribution plots by lattice fringe analysis.

Consistent with the visual representations, there is a minimal change in nanostructure with increase in oxidation pressure. With increasing oxidation pressure, M1300 exhibited a progressive increase in graphitic structure, as observed by a small increase in fringe length and decrease in fringe tortuosity values. R250 still showed a progressive increase in graphitic structure, albeit different burning mode. With increasing pressure, the median fringe length increased and the median fringe tortuosity decreased substantially. OLC showed a decrease in nanostructure order, in agreement with the visual representations where external burning occurred leading to breakup of outer surface lamellae. The diesel soot has little change in fringe length and tortuosity.

XPS results were obtained for each sample to obtain chemical information regarding heteroatom concentration, and sp2/sp3 carbon bonding configurations. Table 4 summarizes the atomic percentages of the elements, and the sp^2/sp^3 values obtained from the C1s peak.

Table 4. Summary of C and O concentration, and carbon bonding by XPS

Sample	C (%)	O (%)	sp^2/sp^3
M1300	98.1	1.9	2
R250	95.8	4.1	2.6
OLC	95.4	4.5	3.4

While oxygen content is typically assumed as a good indicator of oxidative reactivity [19-20], this study showed that the surface atomic concentrations of carbon and oxygen were similar, however the reactivities were different.

Fringe analysis parameters such as fringe length, fringe tortuosity, and sp^2/sp^3 for the different model carbons and reference diesel soot, are plotted against the activation energy values, in order to establish a relation between HRTEM results and the reactivity. Figures 13 and 14 show that as the activation energy value increases, the fringe length and the sp^2/sp^3 ratio increase and the fringe tortuosity decreases. Previous studies have similarly shown a correlation between these nanostructure metrics and oxidation rate [11, 21]. This is consistent with the interpretation of increasing reactivity as reflecting a lower relative fraction of edge site carbon atoms. Another consideration is less C-C bond strain (reflecting lower lamella curvature), effectively increased the activation energy and decreased the oxidation rate.

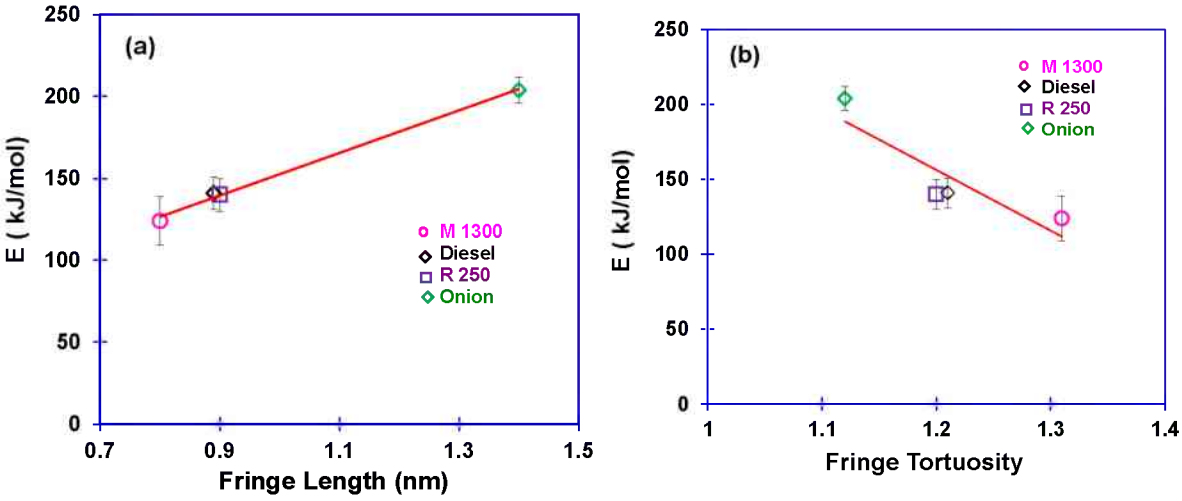

Figure 13. Comparison of the activation energy ratio for different samples with changes in (a) mean fringe Length, (b) mean fringe tortuosity.

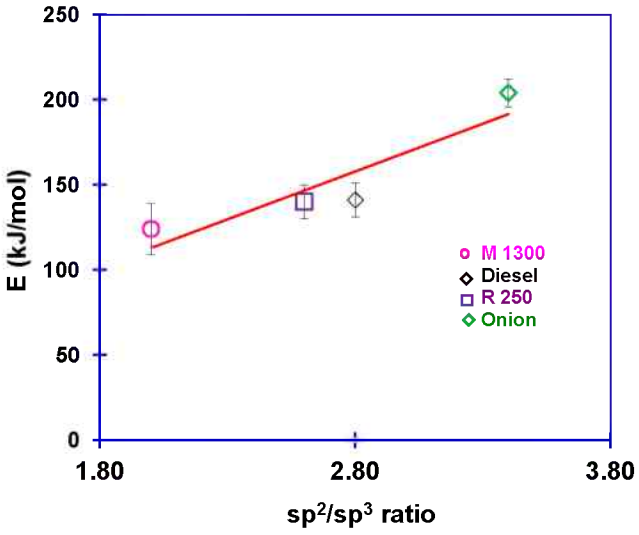

Figure 14. Comparison of the activation energy ratio for different samples with variations in sp^2/sp^3 ratio

Summary

The results of this work can be summarized as:

Oxidation of soot derived from Liquid Fuels

- Isothermal oxidation experiments were conducted in a HP-TGA for soot generated from different liquid fuels and two standards: carboxen and standard reference diesel. Three total pressures were evaluated, 1, 10 and 40 atm., and the O_2 concentration was varied between 10 and 21%. Parameters such as oxidizer flow rate, initial mass loading, and amount of inert bed were optimized in order to ensure that the experiments were carried out under conditions where kinetics control the reaction.

- Even under optimized conditions, mass transfer diffusion limitations influenced the pressurized experiments and corrections based on effectiveness factors were used to account for this.

- There was not a significant difference in the activation energies of the soot samples for either pure components or as a mixture, with exception of soot from oxygen-containing fuels. The activation energies were within the range reported by others.

- Soot nanostructure for the soot collected from the flat flame "nascent", and partially oxidized at 1, 10 and 40 atm was studied by High-Resolution Transmission Electron Microscopy (HRTEM). The lattice fringe length and fringe tortuosity were estimated to correlate the nanostructure and the soot reactivity, and the nascent soot nanostructure was similar across the five fuels. n-butanol/n-dodecane soot showed a significant change in nanostructure with increasing pressure; however, there was no apparent change in the nanostructure (length or tortuosity) for the other fuels.

- Validating the HRTEM data, surface carbon oxidation studies by XPS showed that the sp^2/sp^3 content for the oxygenated fuel blend was 6 times lower than the other fuels leading to lower activation energy and external surface lamellae break-up.

Oxidation of model carbons

- Isothermal oxidation experiments were conducted for three-carbon black and one reference diesel sample. Results showed that the onion-like structure exhibited a slower kinetic rate compared to the amorphous M1300. Similar kinetic parameters were found for R-250 and reference diesel soot samples.

- HRTEM images revealed that the three carbon blacks exhibited different nanostructure in their nascent form. M1300 exhibited mostly partially and completely closed, not spherical but distorted shells. R250 had short, disconnected, individual graphene segments that appear to be oriented concentrically but the inner core was disorganized. OLC exhibited extended carbon lamella, many parallel to each other. Dissimilar to the model carbons, the reference diesel soot showed typical core shell structure.

- HRTEM images with increasing oxidative pressure showed a significant change in nanostructure relative to the nascent structure. Both the nascent material nanostructure and pressure played a role in the observed changes. This observation may be caused by mass transfer diffusion limitations which were found to affect the pressurized experiments.

- The fringe analysis explained the differences in the kinetic parameters between the carbon samples studied. The OLC nascent sample had a longer range of fringe lengths and smaller tortuosity, suggesting a flatter structure; the nascent M1300, had much shorter fringe length and broader tortuosity, suggesting more curvature. The nascent R250 and diesel sample were between the other two carbons. A linear correlation between the image analysis and XPS data was found. Results showed that as the sp^2/sp^3 ratio increased, the fringe length increased. In contrast, as the sp^2/sp^3 ratio increased, the fringe tortuosity decreased.

References

[1] P. Ciambelli, P. Corbo, M. Gambino, V. Palma, S. Vaccaro, Catal. Today 27 (1996) 99–106.
[2] K. Otto, M. Sieg, M. Zinbo, L. Bartosiewicz, SAE Tech. Pap. 800336, (1980).
[3] J. P. Neeft, T. X. Nijhuis, E. Smakman, M. Makkee, J. A. Moulijn, Fuel 76 (1997) 1129–1136.
[4] N. Miyamoto, Z. Hou, H. Ogawa, SAE Tech. Pap. 881224, (1988).
[5] P. Gilot, F. Bonnefoy, F. Marcuccilli, G. Prado, Combust. Flame 95 (1993) 87–100.
[6] K. J. Higgins, H. Jung, D. B. Kittelson, J. T. Roberst, M. R. Zachariah, Phys. Chem. A. 106 (2002) 96-103.
[7] J. Song, M. Alam, A.L. Boehman, Combust. Sci. and Tech. 179 (2007) 1991-2037.
[8] M. Kalogirou, Z. Samaras, J. Therm. Anal. Calorim. 98 (2009) 215–224.
[9] L. H. Sorensen, E. Gjernes, T. Jessen, J. Fjellerup, Fuel 75 (1996) 31–38.
[10] T. Ishiguro, Y. Takatori, K. Akihama, Combust. Flame 108 (1997) 231–234.
[11] R.L. Vander Wal, A.J. Tomasek, Combust. Flame 134 (2003) 1–9.
[12] R.L. Vander Wal, V.M. Bryg, M.D. Hays, Anal. Chem. 83 (2011) 1924–1930.
[13] B.R. Stanmore, J. Brilhac, P. Gilot, Carbon 39 (2001) 2247–2268.
[14] B. Stanmore, P. Gilot, G. Prado, Thermochim. Acta 240 (1994) 79–89.
[15] K.J. Higgins, H. Jung, D.B. Kittelson, J.T. Roberts, M.R. Zachariah, Environ. Sci. Technol 37 (2003) 1949–1954.
[16] T. Ishiguro, N. Suzuki, Y. Fujitani, H. Morimoto, Combust. Flame 85 (1–2) (1991) 1–6.
[17] R.L. Vander Wal, A. Yezerets, N.W. Currier, D.H. Kim, C.M. Wang, Carbon 45 (2007) 70–77.
[18] K. Al-Qurashi, A.L. Boehman, Combust. Flame 155 (2008) 675–695.
[19] G. de la Puente, E. Fuente, J.J. Pis, J. Anal. Appl. Pyrol. 53 (2000) 81-93.
[20] H.J. Seong, A.L. Boehman, Energy & fuels 25 (2011) 602–616.
[21] J. Song, M. Alam, A.L. Boehman, U. Kim, Combust. Flame 146 (2006) 589–604.

Publications

Papers and Presentations from July 1, 013 to June 30, 2014 (anticipated).

- I. Jaramillo, C. K. Gaddam, R. Vander Wal, and J. S. Lighty, "Oxidation Kinetics and nanostructure of model carbons," in preparation for Combustion and Flame (2014).

- I. Jaramillo, C. K. Gaddam, R. L. VanderWal, C-H Huang, J. D. Levinthal, and J. S. Lighty, "Soot oxidation kinetics under pressurized conditions," in revision, Combustion and Flame (2013).

Contributions to:

- P. Toth, J. K. Farrer, A. B. Palotas, J. S. Lighty, E. G. Eddings, "Automated analysis of heterogeneous carbon nanostructures by high-resolution electron microscopy and on-line image processing," Ultramicroscopy, 129, 53-62 (2013). Featured on cover.

- P. Toth, A. B. Palotas, T. A. Ring, E. G. Eddings, R. Vander Wal, C. K. Gaddam, J. Levinthal, I.C. Jaramillo, and J. S. Lighty, "Detailed investigation of soot nanostructure: effect of pressure," in preparation.

Presentations

- J. D. Levinthal, C. Jaramillo, C. K. Gaddam and R. Vander Wal, and J. S. Lighty, "Oxidation Behavior of Biodiesel Surrogate Soot: Examination using X-Ray Photoelectron Spectroscopy (XPS), HR-TEM and Thermogravimetric Analysis (TGA)," presented at the 2013 Annual AIChE Meeting, San Francisco, CA (2013).

- I. C. Jaramillo, J. Levinthal, C. K. Gaddam, R. Vander Wal, and J. Lighty, "Oxidation kinetics and nanostructure of model carbons based on high pressure TGA data," presented at the 8th US National Meeting of the Combustion Institute, Canyons, UT, May (2013).

- P. Toth, A. B. Palotas, T. A. Ring, E. G. Eddings, R. Vander Wal, C. K. Gaddam, J. Levinthal, I.C. Jaramillo, and J. S. Lighty, "Detailed investigation of soot nanostructure: effect of pressure," presented at the 8th US National Meeting of the Combustion Institute, Canyons, UT, May (2013).

- C.K. Gaddam, R.L. Vander Wal, J.D. Levinthal, I.C. Jaramillo, J.S. Lighty, "Impact of nanostructure on soot oxidation: Pressure and fuel comparisons," Presented at the ACS 246th National Meeting & Exposition, Indianapolis, IN, September (2013).